Available online at www.sciencedirect.com
SCIENCE DIRECT®
Journal of Power Sources 119–121 (2003) 727–732
JOURNAL OF POWER SOURCES
www.elsevier.com/locate/jpowsour

Structure transformation of $LiAl_{0.15}Mn_{1.85}O_4$ cathode material during charging and discharging in aqueous solution

Bing-Joe Hwang[a,*], Yin-Wen Tsai[a], Raman Santhanam[a], Shao-Kang Hu[b], Hwo-Shuenn Sheu[c]

[a] *Microelectrochemistry Laboratory, Department of Chemical Engineering, National Taiwan University of Science and Technology, 43, Keelung Road, Sec. 4, Taipei 106, Taiwan, ROC*
[b] *Department of Chemical Engineering, National Cheng Kung University, Tainan 701, Taiwan, ROC*
[c] *National Synchrotron Radiation Research Center, 1 R&D Road VI, Hsinchu Science-Based Industrial Park, Hsinchu 300, Taiwan, ROC*

Abstract

The electrochemical lithium-ion extraction/insertion properties of a spinel $LiAl_{0.15}Mn_{1.85}O_4$ material were studied. Cyclic voltammetry shows two-step reactions for lithium-ion extraction/insertion at its 4 V plateau. Synchrotron in situ X-ray diffraction studies show that lithium ions are extracted and inserted from the $LiAl_{0.15}Mn_{1.85}O_4$ material, respectively, from two to three different environments. The different environments may be due to different Li–Li interactions and/or different intensities of interactions with the nearest neighbors in the spinel $LiAl_{0.15}Mn_{1.85}O_4$ material frame work. From the Mn absorption edge measurements as a function of potential, during lithium extraction, it can be suggested that the charge transfer rate is faster than that of structural transformations. However, during lithium insertion, the rate of both charge transfer and structural transformations are more or less similar.

Keywords: $LiMn_2O_4$; Al-substitution; Phase transitions; In situ X-ray diffraction

1. Introduction

$LiMn_2O_4$ cathode has been suggested as a commercially viable alternative to the current nickel and cobalt based systems due to their easy preparation, low cost, high specific energy and low toxicity [1–4]. However, $LiMn_2O_4$ exhibits severe capacity fading during electrochemical cycling. This capacity fading is ascribed to several possible factors: (i) the decomposition of the electrolyte at higher potentials [5,6], (ii) a slow dissolution of Mn from active cathode material to the electrolyte via the disproportionation reaction [7], $2Mn^{3+} \rightarrow Mn^{2+} + Mn^{4+}$, (iii) the Jahn–Teller distortion at the deeply discharged state [8], (iv) site exchange between Li and Mn [9], and so on. Various modifications in order to improve the battery performance of the $LiMn_2O_4$ spinel material have been reported [10–15].

Because of the water oxidation problem in aqueous electrolyte, most of the studies on the $LiMn_2O_4$ cathode material for rechargeable batteries were carried out in non-aqueous electrolytes. Martin and co-worker's recent work [16] on nanostructured $LiMn_2O_4$, which showed high rate capability, in aqueous solution stimulated us to investigate the structural changes of spinel $LiMn_2O_4$ in aqueous solution. Among the modifications of $LiMn_2O_4$ spinel material, one approach is the substitution of Mn by metal ions which may stabilize its structure. Ceder et al. reported that Al doping is potentially attractive for electrochemical applications because of the higher intercalation voltage, higher energy density and lower cost although it still shows capacity fading to some extent during the course of cycling [17]. Accordingly, we have synthesized Al-substituted $LiMn_2O_4$ in this work.

It has been reported that the phase transitions would affect the capacity retention of the cathode materials during the charging/discharging process. Earlier ex situ X-ray diffraction studies of $LiMn_2O_4$ were performed by Ohzuku et al. [18]. They proposed a two-phase model in which spinel $Li_xMn_2O_4$ undergoes a phase transition to the empty spinel Mn_2O_4 (λ-MnO_2). Liu et al. [19] proposed a three-phase model: from single-phase A ($0 < x < 0.2$) to a two-phase coexistence region A + B ($0.2 < x < 0.4$), to a single-phase B ($0.45 < x < 0.55$), and finally to a single-phase C ($0.55 < x < 1$). This three-phase model is interesting and different from the two-phase system proposed by Ohzuku et al. [18]. Recently, Sun et al. [20] demonstrated a three-phase model with two

* Corresponding author. Tel.: +886-2-27376624; fax: +886-2-27376644.
E-mail address: bjh@ch.ntust.edu.tw (B.-J. Hwang).

0378-7753/03/$ – see front matter © 2003 Published by Elsevier Science B.V.
doi:10.1016/S0378-7753(03)00211-8

two-phase coexistence between cubic phases (A and B) and (B and C). All the above studies have been carried out on $Li_xMn_2O_4$ spinel materials in non-aqueous solutions. To our knowledge, no studies have been reported on the structural changes of Al-substituted $LiMn_2O_4$ that occur during charging and discharging in aqueous solution. In this work, using a synchrotron based, in situ X-ray diffraction technique, the structural changes of $LiAl_{0.15}Mn_{1.85}O_4$ material have been studied during charge and discharge cycling. The results during first charge and discharge are reported in this work.

2. Experimental

$LiAl_{0.15}Mn_{1.85}O_4$ spinel material was synthesized using citric acid as a chelating agent, as described in our previous reports [10,21]. Stoichiometric amounts of lithium acetate ($Li(CH_3COO)\cdot 4H_2O$), manganese acetate ($Mn(CH_3COO)_2\cdot 4H_2O$), and aluminum nitrate ($Al(NO_3)_3\cdot 9H_2O$) were dissolved in distilled water into which citric acid was added dropwise with continuous stirring. The solution pH was adjusted to 6.0 using ammonium hydroxide and the temperature was maintained at 35 °C. The prepared solution was then heated in a beaker on a hot plate to 80–90 °C and maintained for 4 h until a transparent sol was obtained. The resulting gel precursor was decomposed at 400 ° for 4 h in oxygen to remove the organic contents. Finally, the precursor was ground to a fine powder and calcined at 800 °C in oxygen for 10 h with a heating rate of 2 °C/min.

Cathodes were prepared by mixing the active material, carbon black, KS6 graphite and polyvinylidene fluoride binder at a ratio of 80:3.5:1.5:10 (w/w) in *N*-methyl pyrrolidinone. The resulting paste was coated onto an aluminum current collector. The entire assembly was dried under vacuum overnight and then heated in an oven at 120 °C for 2 h. For cyclic voltammetry and X-ray absorption spectroscopy measurements, a three-electrode cell with a $LiAl_{0.15}Mn_{1.85}O_4$ working electrode, platinum foil as the counter electrode and a saturated calomel electrode (SCE) reference electrode was employed. Although a SCE reference was used, all voltages are reported here versus Li/Li^+ (0 V versus SCE corresponding to 3.283 V versus Li/Li^+). A saturated aqueous solution $LiNO_3$ (9.0 M) was used as the electrolyte.

Investigation of in situ XRD patterns for the $LiAl_{0.15}Mn_{1.85}O_4$ material was performed using the synchrotron radiation light source with a wavelength of $\lambda = 1.32633$ Å on the beam line BL17A at NSRRC in Taiwan. A single crystal of Si(1 1 1) was used as a monochromator to adjust the light energy into the hutch. The photon flux (energy 9 keV, exposure time, 10 min) is concerned more than resolution at the beam line BL17A. The optics are designed to focus the beam into a 0.1 mm × 3 mm spot size at the sample position. A flat imaging plane (Fuji, 20 cm × 40 cm) was used as a 2-D area detector, which can collect all of the in situ XRD patterns. The diffraction pattern is read out by using a MAC IPR420 off line imaging plate scanner and the step size was 0.02 for the 2θ scan.

3. Results and discussion

The charge and discharge reactions for $LiMn_2O_4$ in the 4 V plateau region can be represented by the following equation:

$$LiMn_2O_4 \Leftrightarrow Li_{1-x}Mn_2O_4 + xLi^+ + xe^- \ (0 \le x \le 1)$$

During charging, the Li^+ ions deinserted from $LiMn_2O_4$ would come into the electrolyte solution and these ions are stable in concentrated $LiNO_3$ (9.0 M) electrolyte solution [22]. Hence, the Li^+ ions presented in the solution would insert into $LiMn_2O_4$ electrode material during discharging. The electrolysis of water occurs on the Pt counter electrode during charging and discharging.

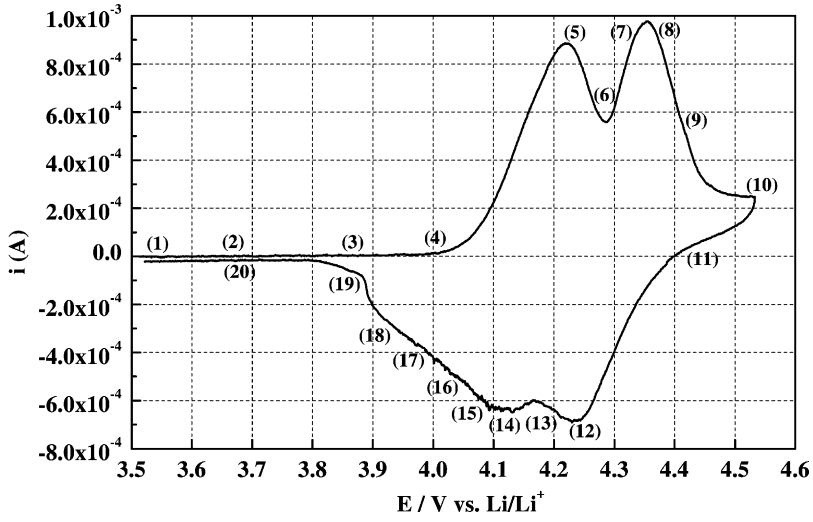

Fig. 1. Cyclic voltammogram of $LiAl_{0.15}Mn_{1.85}O_4$ in 9.0 M $LiNO_3$ aqueous solution at a scan rate of 0.05 mV s^{-1}.

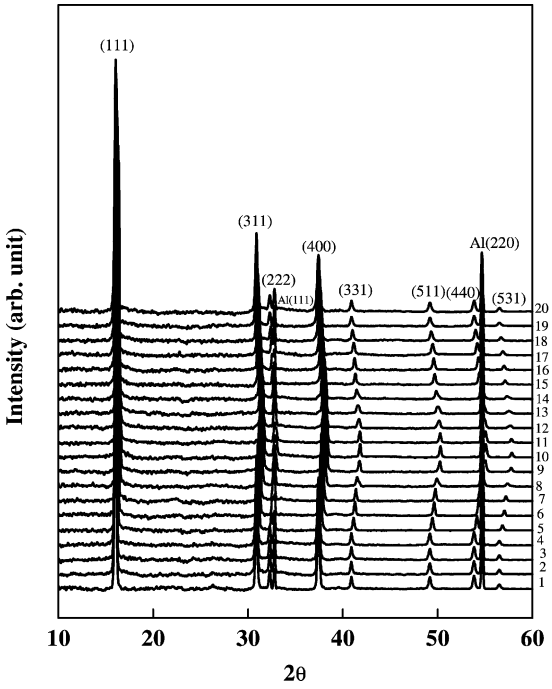

Fig. 2. In situ XRD patterns ($2\theta = 10$–60°) of $LiAl_{0.15}Mn_{1.85}O_4$ cathode material during the first charge and discharge scan between the potential range of 3.5 and 4.6 V.

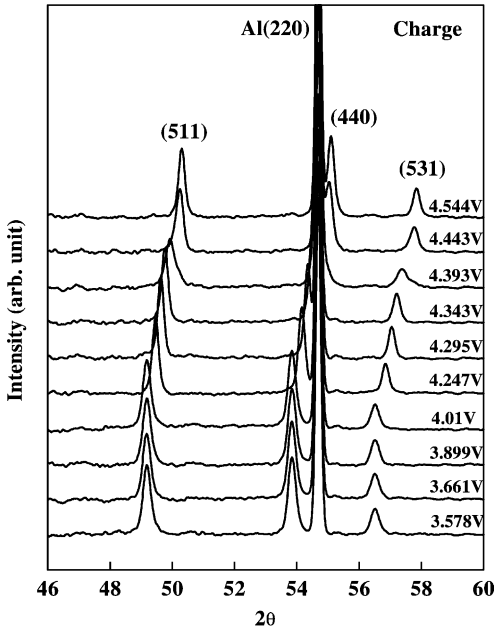

Fig. 3. In situ patterns ($2\theta = 46$–60°) of $LiAl_{0.15}Mn_{1.85}O_4$ cathode material during charge between the potential range of 3.5 and 4.6 V.

Cyclic voltammetry experiments were performed by scanning over the potential range between 3.5 and 4.6 V (forward, charge scan and reverse, discharge scan) in 9.0 M aqueous $LiNO_3$ solution. Fig. 1 shows the cyclic voltammograms for the $LiAl_{0.15}Mn_{1.85}O_4$ electrode at a scan rate of 0.05 mV s^{-1}. Over this potential window, two voltammetric waves can be observed indicating that the material undergoes phase changes during the intercalation process [17,21]. It has already been established that the lower potential wave (centered at 4.22 V) is attributed to the removal of lithium ions from half of the tetrahedral sites at which Li–Li interaction occurs. The high potential wave (centered at 4.35 V) is due to the removal of lithium ions from the rest of the tetrahedral sites at which Li ions do not have Li–Li interactions [23]. It is interesting to note that the potential difference (ΔE_p) between these two redox peaks was larger than the reversible value, 60 mV. In contrast, the ΔE_p value was smaller than 60 mV in non-aqueous electrolyte [10]. The larger ΔE_p value observed in aqueous solution was caused by concentration polarization and slow electron transfer [4].

The structural transformation of $LiAl_{0.15}Mn_{1.85}O_4$ cathode material was studied by in situ XRD measurement using the synchrotron radiation light source with a wavelength of $\lambda = 1.32633$ Å. Fig. 2 displays in situ XRD patterns of

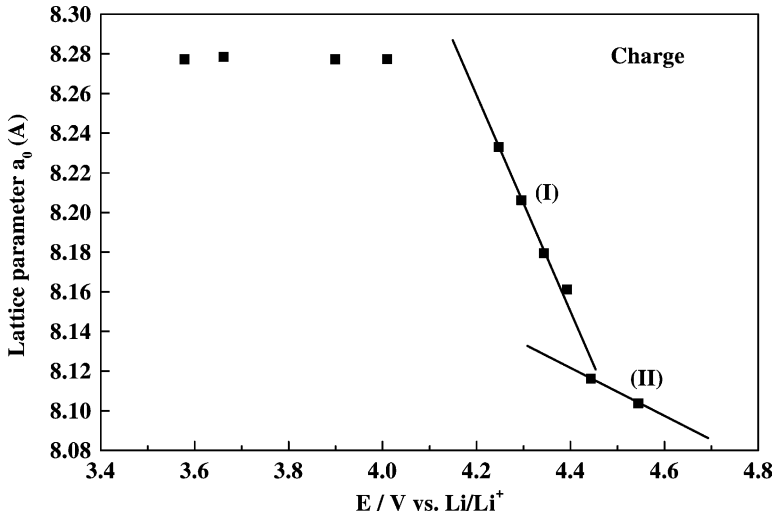

Fig. 4. Variation of lattice parameter (a_0) of $LiAl_{0.15}Mn_{1.85}O_4$ cathode material during charge as a function potential between 3.5 and 4.6 V.

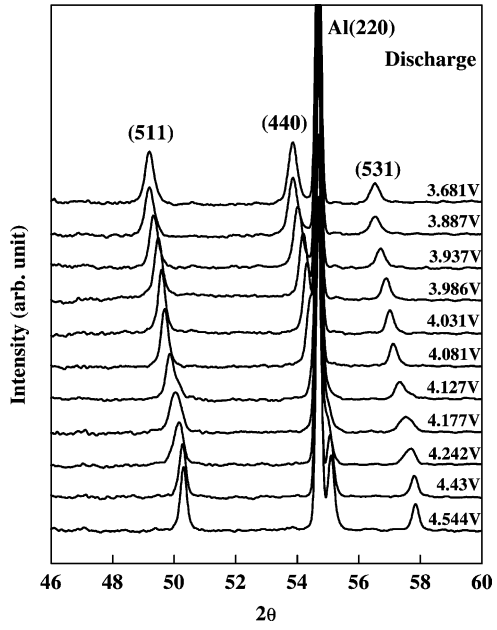

Fig. 5. In situ patterns of $LiAl_{0.15}Mn_{1.85}O_4$ cathode material during discharge between the potential range of 3.5 and 4.6 V.

$LiAl_{0.15}Mn_{1.85}O_4$ cathode material during the first charge and discharge scan between the potential range of 3.5 and 4.6 V. The scan numbers marked in Fig. 2 correspond to the numbers marked on the cyclic voltammetric curve in Fig. 1. Structural determination of $LiAl_{0.15}Mn_{1.85}O_4$ results in a single-phase of cubic spinel with a space group *Fd*3*m* where Li(1/8, 1/8, 1/8) occupied the 8a sites, Mn(1/2, 1/2, 1/2) and Al(1/2, 1/2, 1/2) occupied the 16d sites, and O(*X*, *X*, *X*) occupied the 32e site. All the diffraction peaks of $LiAl_{0.15}Mn_{1.85}O_4$ are observed to shift to higher 2θ while the potential scanning is positive to proceed an oxidation reaction. In contrast, the peaks are back to lower 2θ while the potential scanning is negative to have a reduction reaction. The expanded spectra of (5 1 1), (4 0 0) and (5 3 1) peaks during the first charge from 3.5 to 4.6 V are shown in Fig. 3. We found that the peak broadening process occurs at 4.393 V versus Li from the variation of (5 3 1) diffraction peaks. Generally, the broadening of the Bragg peak could result either from the overlap of two peaks or a decrease of grain size. The broadening at 4.393 V versus Li is apparently due to the overlap of the two peaks. The variations of lattice parameters a_0 of $LiAl_{0.15}Mn_{1.85}O_4$ during the charge process are shown in Fig. 4. The lattice parameter, a_0, decreases with increasing oxidation potential due to extraction of lithium ions from the tetrahedral site of the spinel framework. During charging, two different slopes (I) and (II), indicating two different phases, are observed (Fig. 4) which represent different extraction rate of Li from the tetrahedral site. The Li extraction rate is faster in slope (I) than in slope (II). It may be due to the intensity of interaction on Li with the nearest neighbors of spinel the $LiAl_{0.15}Mn_{1.85}O_4$ frame work. As seen in Fig. 4, the intensity of the interaction is weaker in slope (I) than in the slope (II) region. The transition point of the slope change occurs at the potential of 4.45 V. This point seems to be a two-phase coexistence region. It is expected that the variation in Li extraction rate of the Al-substituted spinel would certainly cause structural changes. Fig. 5 shows the expand spectra of (5 1 1), (4 0 0) and (5 3 1) peaks during the first discharge from 4.6 to 3.5 V. The peak broadening process occurs at 4.242, 4.177 and 4.127 V versus Li. The variations of lattice parameters, a_0, of $LiAl_{0.15}Mn_{1.85}O_4$ during the discharge process are shown in Fig. 6. Three different types of slopes (I), (II) and (III) are observed in this figure. Two transition points of the slope change are observed at 4.15 and 4.32 V, respectively. This observation indicates three different environments around Li, which may be either different Li–Li interaction or different intensities

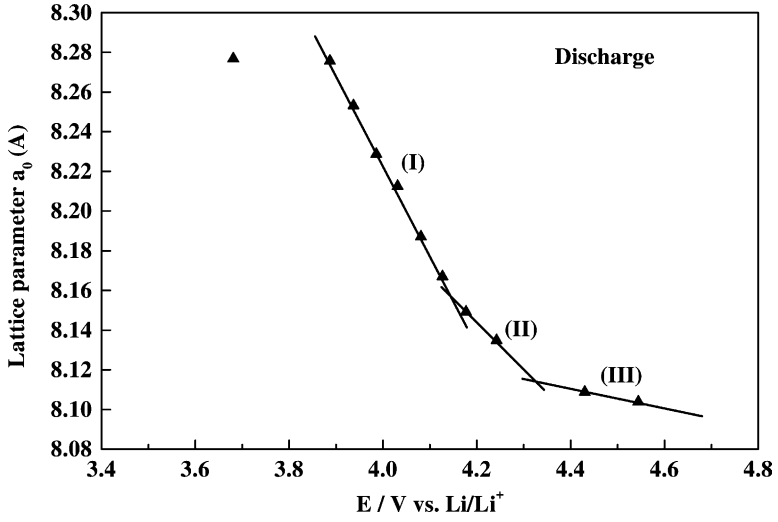

Fig. 6. Variation of lattice parameter (a_0) of $LiAl_{0.15}Mn_{1.85}O_4$ cathode material during discharge as a function potential between 3.5 and 4.6 V.

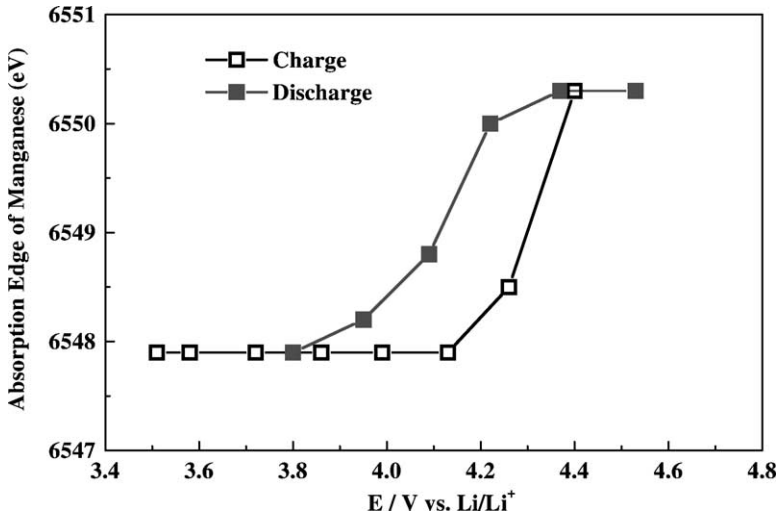

Fig. 7. Variation of manganese absorption edge of $LiAl_{0.15}Mn_{1.85}O_4$ cathode material during charge and discharge as a function potential between 3.5 and 4.6 V.

of interaction of Li with the nearest neighbors. Fig. 7 shows the variation of absorption edge as a function of potential during lithium-ion extraction/insertion. It is clear from this figure that the Mn oxidation is almost completed at 4.4 V and reduction is completed around 3.8 V. However, the lattice parameter continues to change significantly after 4.4 V also during lithium extraction (Fig. 4). This observation reveals that the rate of charge transfer is faster than that of structural transformations during charge. The potential observed for the completion of Mn reduction (Fig. 7) and for the completion of structural transformation (Fig. 6) are almost similar during lithium insertion. This means that both Mn reduction and structural transformation occur in a similar rate during discharge.

4. Conclusions

The structural changes of a spinel $LiAl_{0.15}Mn_{1.85}O_4$ material were investigated during charge and discharge in aqueous solution. From in situ XRD data and the plot of lattice parameter versus potential, two and three different slopes are observed, respectively, during lithium extraction (charging) and lithium insertion (discharging). These observations indicate that lithium is extracted from the $LiAl_{0.15}Mn_{1.85}O_4$ material from two different environments and inserted into the material in three different environments. The different environments may be due to different Li–Li interactions and/or different intensities of interaction with the nearest neighbors in the spinel $LiAl_{0.15}Mn_{1.85}O_4$ material framework. From the Mn absorption edge measurements as a function of potential, during lithium extraction, it is found that the charge transfer rate is faster than that of structural transformations. However, during lithium insertion, the rate of both charge transfer and structural transformations are more or less similar.

Acknowledgements

The financial support from National Science Council (NSC 89-2214-E-011-044- and NSC 90-2811-ET-AL-011-005-) and Education Ministry (EX-91-E-FA09-5-4), National Synchrotron Radiation Research Center (NSRRC), Hsinchu and National Taiwan University of Science and Technology, Taiwan, Republic of China, is gratefully acknowledged.

References

[1] C. Sigala, D. Guyomard, A. Vebaere, Y. Piffard, M. Tournoux, Solid State Ionics 81 (1995) 167.
[2] Y. Xia, M. Yoshio, J. Power Sources 56 (1995) 61.
[3] J.M. Tarascon, D. Guyomard, Electrochim. Acta 38 (1993) 1221.
[4] J.M. Tarascon, E. Wang, F.K. Sholooki, W.R. Mckinnon, S.J. Colson, Electrochem. Soc. 138 (1991) 2859.
[5] D. Guyomard, J.M. Tarascon, J. Electrochem. Soc. 139 (1992) 937.
[6] R.J. Gummow, A. de Kock, M.M. Thackeray, Solid State Ionics 69 (1994) 59.
[7] D.H. Jang, Y.J. Shin, S.M. Oh, J. Electrochem. Soc. 143 (1996) 2204.
[8] M.M. Thackeray, Y. Shao-Horn, A.J. Kahainan, K.D. Kepler, E. Skinner, J.T. Vaughey, S.A. Hackney, Electrochem. Solid-State Lett. 1 (1998) 7.
[9] J.M. Tarascon, W.R. Mckinnon, F. Coowar, T.N. Bowmer, G. Amatucci, D. Guyomard, J. Electrochem. Soc. 141 (1994) 1421.
[10] B.J. Hwang, R. Santhanam, D.G. Liu, Y.W. Tsai, J. Power Sources 102 (2001) 326.
[11] A. Momchilov, V. Manev, A. Nassalevska, J. Power Sources 41 (1993) 305.
[12] R.J. Gummow, M.M. Thackeray, J. Electrochem. Soc. 141 (1994) 1178.
[13] Y. Xia, Y. Zhou, M. Yoshio, J. Electrochem. Soc. 144 (1997) 2593.
[14] A. Amacucci, A. Du Pasquier, A. Blyr, T. Zheng, J.M. Tarascon, Electrochim. Acta 45 (1999) 255.
[15] Y.K. Sun, Y.S. Jeon, H.J. Lee, Electrochem. Solid-State Lett. 3 (2000) 7.
[16] N. Li, C.J. Patrissi, G. Che, C.R. Martin, J. Electrochem. Soc. 147 (2000) 2044.

[17] G. Ceder, Y.M. Chiang, D.R. Sadoway, M.K. Aydinol, Y.I. Jang, B. Huang, Nature 392 (1998) 694.
[18] T. Ohzuku, M. Kitagawa, T. Hirai, J. Electrochem. Soc. 137 (1990) 769.
[19] W. Liu, K. Kowal, G.C. Farrington, J. Electrochem. Soc. 145 (1998) 459.
[20] X. Sun, X.Q. Yang, M. Balasubramanian, J. McBreen, Y. Xia, T. Sakai, J. Electrochem. Soc. 149 (2002) A842.
[21] B.J. Hwang, R. Santhanam, D.G. Liu, J. Power Sources 101 (2001) 86.
[22] W. Li, J.R. Dahn, D.S. Wainwright, Science 264 (9) (1994) 1115.
[23] T. Ohzuku, M. Kitagawa, T. Hirai, Nature 137 (1990) 769.